ORIGINAL ARTICLE

A Robust Data Evaluation Method for the DCMIX Microgravity Experiments

D. Sommermann[1] · T. Triller[1] · W. Köhler[1] (ORCID)

Abstract

Measurements of non-isothermal diffusion in ternary mixtures under microgravity conditions are performed in the framework of the DCMIX (Diffusion and thermodiffusion Coefficient Measurements in ternary mIXtures) project aboard the ISS by means of the SODI instrument. Its digital Mach-Zehnder interferometer permits the time resolved determination of the 2d-refractive index profile within a Soret cell at two different detection wavelengths of 670 and 935 nm. The operation of the interferometer is based on temporal phase stepping, where five consecutive images with a phase shift of $\pi/2$ are combined to an image stack. We present a robust method for the evaluation of these interferometric data by mapping the time evolution of the phase gradient in the center of the cell to an equivalent two-color optical beam deflection (2-OBD) experiment. It allows to extract transients of the central phase gradient even in occasional situations where temporal phase stepping breaks down due to laser instabilities. For this purpose, only a single image from every image stack, instead of five images with well controlled $\pi/2$-phase stepping, is required. Our results demonstrate the sound design and the robustness of the SODI instrument, which still yields fully valid data even in the event of unexpected laser phase instabilities.

Introduction

In a typical Soret experiment, a temperature gradient is applied to an initially homogeneous and isothermal fluid, and the evolution of a composition gradient is then monitored as a function of time. Eventually, a steady state is reached, where the composition gradient is determined by the balance of the counteracting Fickian diffusion and thermodiffusion. The proportionality constant between the temperature gradient and the concentration gradient of species i is the corresponding Soret coefficient $S'_{T,i}$:

$$\nabla c_i = -S'_{T,i} \nabla T \tag{1}$$

✉ W. Köhler
werner.koehler@uni-bayreuth.de

1 Physikalisches Institut, Universität Bayreuth, 95440, Bayreuth, Germany

Unexpected convection can cause serious problems in Soret cell experiments with a quiescent multicomponent fluid. The onset of thermosolutal instabilities in such systems has been described in detail in the pioneering book on convection in liquids by Platten and Legros (1984). In particular the triple-diffusive ternary mixtures (Pearlstein et al. 1989) are much more complicated than binaries. Even in a presumably stable configuration, slight asymmetries or misalignments of the sample cell with respect to gravity can result in dangerous slow convective currents that are difficult to spot in the experiment but distort the results. The need to identify and avoid such problems and to perform Soret coefficient measurements in microgravity was clearly recognized by Legros, who quickly became a leading figure in the development of microgravity experiments on liquid mixtures (Van Vaerenbergh and Legros 1998; Van Vaerenbergh et al. 1995; Vaerenbergh et al. 1998; Touzet et al. 2011).

By carefully avoiding convection problems, reliable experimental techniques have been developed for binary mixtures, and the base of trustworthy data has steadily grown over the past decades (Wiegand 2004; Köhler and Morozov 2016). Much less is known about thermodiffusion in ternary mixtures (Mounir and Platten 2005), whose

investigation has gained momentum only very recently, mainly driven by the activities within the DCMIX (Diffusion and thermodiffusion Coefficient Measurements in ternary mIXtures) project (Shevtsova et al. 2011; Mialdun et al. 2013; Bou-Ali et al. 2015; Triller et al. 2018). This project of ESA and Roscosmos comprises a series of so-far four microgravity measurement campaigns for the investigation of diffusion and thermodiffusion of ternary mixtures aboard the International Space Station (ISS).

The DCMIX experiments are performed in the Selectable Optical Diagnostics Instrument (SODI), a two-color Mach-Zehnder interferometer that is permanently stored on the ISS and set up in the Microgravity Science Glovebox (MSG) for the duration of the measurements. Only the cell array with five ternary mixtures and a binary one is delivered to the ISS with an unmanned transport vehicle. After completion of the experiments, SODI is disassembled and stowed away, the cell array is discarded and the hard disks with the data are returned to ground for processing. The microgravity measurements of three out of the four campaigns have already been completed: DCMIX1 in 2012, DCMIX2 in 2014 and DCMIX3 in 2016. A number of publications have emerged from these experiments (Khlybov et al. 2015; Mialdun et al. 2015; Galand and Van Vaerenbergh 2015; Ahadi and Ziad Saghir 2015; de Mezquia et al. 2015; Jurado et al. 2016, 2018; Ollé et al. 2017; Mialdun et al. 2018; Gebhardt and Köhler 2015a; Legros et al. 2015; Triller et al. 2018), but the data evaluation is still going on. The experiments of the fourth campaign, DCMIX4, were carried out from the end of 2018 until early 2019.

The SODI instrument employs temporal phase-stepping interferometry, where an image stack composed of five phase-shifted images is collected at every instance in time. A full 2d-phase map of the Soret cell can be reconstructed from every single stack (Mialdun et al. 2015). Khlybov et al. have applied an alternative Fourier transform method, by which a phase image can be obtained from a single interference image, rather than an entire image stack, after subtraction of the refractive index offset and removal of the carrier frequency (Khlybov et al. 2015). A recent benchmark, for cell 3 of DCMIX1, containing a mixture of tetralin/isobutylbenzene/n-dodecane at 0.8/0.1/0.1 mass fractions, showed a good agreement between different data evaluation schemes and also a good agreement between the microgravity and laboratory results (Bou-Ali et al. 2015; Khlybov et al. 2015; Mialdun et al. 2015; Galand and Van Vaerenbergh 2015; Ahadi and Ziad Saghir 2015; Larrañaga et al. 2015).

There is, however, not only light but also shadow: the lasers built into SODI suffer from occasional instabilities, which cannot be fixed in space and render temporal phase stepping of the affected image stacks useless. Additionally,

there was some misalignment of the cell array during DCMIX3 (Triller et al. 2018), which lead to five percent of the image of cell 1 and three percent of the image of cell 2 missing the camera sensor. In this contribution we will show that the experimental design of SODI/DCMIX is quite robust and that it is possible to extract unambiguous information even under these unfavorable circumstances. We will do so by extracting the phase gradient only around the center of the cell on a single-image basis without resorting to temporal phase-stepping directly from the fringe pattern. The time series composed of these central phase gradients can then be evaluated in analogy to two-color optical beam deflection (2-OBD) signals.

Experiment

The SODI instrument consists of two Mach-Zehnder interferometers. One is fixed and equipped with a single laser (fixed red, FR, 670 nm). It is used to measure the reference cell containing a binary mixture. The second interferometer is movable and can address the five cells with the ternary mixtures using two different wavelengths (moving red, MR, 670 and moving near-infrared, MN, 935 nm). The compositions of the samples in the five ternary and in the binary DCMIX3 cells are listed in Table 1.

The sample cell has a volume of $10 \times 10 \times 5 \ mm^3$, where the 5 mm are in the direction of the temperature gradient. The applied temperature difference is typically 5 K. The slight tilt of the mirrors, the temperature gradient and the subsequent concentration gradient lead to fringes in the interferogram that are recorded by a CCD camera with an image size of $1920 \times 1080 \ pixel^2$.

In order to translate the fringe images to a 2d-phase image, five images with an image-to-image phase shift of $\pi/2$ are combined in a so-called image stack. The phase shifts are accomplished by current-tuning of the laser. From every image stack a phase image can be constructed. A more detailed description of the experiments can be found in Refs. Triller et al. (2018, 2019), Ahadi et al. (2013), and Shevtsova et al. (2014).

Results and Discussion

Temporal Phase Stepping

Before we will come to our alternative approach, the standard temporal phase-stepping and data evaluation technique shall briefly be recalled. The examples are all from the DCMIX3 campaign for the ternary system water/ethanol/triethylene glycol (H_2O/EtOH/TEG) (Triller et al. 2018).

Table 1 Sample compositions in the five ternary DCMIX3 cells and the binary companion cell (cell 6). All concentrations in mass fractions

Cell	1	2	3	4	5	6
c_{H_2O}	0.20	0.33	0.25	0.75	0.50	0.85
c_{EtOH}	0.20	0.33	0.60	0.15	0.10	0.15
c_{TEG}	0.60	0.33	0.15	0.10	0.40	0.00

Figure 1 shows an image stack with the raw images before proper rotation and cropping to the sample cell. The individual data evaluation steps are illustrated in Fig. 2 for one particular column marked in Fig. 1 by a vertical line. The fringes of the five images from the stack are phase-shifted evenly by $\pi/2$. From these five sinusoidal fringes, the phase, which is still wrapped into the $(-\pi, \pi]$-interval, is computed for every pixel by means of a modified Hariharan algorithm (Mialdun et al. 2015; Kreis 2005; Triller 2018). After unwrapping, the final phase image is obtained, as shown in Fig. 1 for the entire image and in Fig. 2 for the selected column.

There are different possibilities for the evaluation of the phase images by fitting, e.g., the entire 2d-phase profile (Mialdun et al. 2015) or the phase difference between the hot and the cold plate (Galand and Van Vaerenbergh 2015; Ahadi and Ziad Saghir 2015). In our laboratory, we have developed a protocol, where the phase or refractive index gradient in the center of the SODI cell is determined by fitting a suitable polynomial to the unwrapped phase along the y-direction. For noise reduction, the fit result is averaged over several hundred columns to the left and the right of the symmetry axis, thereby avoiding the inhomogeneities of the temperature gradient near the edges. By taking the refractive index gradient in the center of the cell, the SODI experiment can directly be mapped onto 2-OBD experiments, where the refractive index gradient in the center of a similar Soret cell is sensed by deflection of two laser beams of different wavelengths. By this mapping, the treatment of SODI experiments becomes more or less straight forward.

The evaluation of such 2-OBD measurements has been explained in detail in Refs. Haugen and Firoozabadi (2006) and Gebhardt and Köhler (2015b, c). The beam deflection is directly proportional to the central refractive index gradient and contains three time constants. A fast contribution stemming from the temperature gradient and two slower modes corresponding to the two eigenvalues of the diffusion matrix. After normalization to the amplitude of the thermal signal $A_{th,i}$, the time dependence of the OBD-signal measured with wavelength λ_i is given by Gebhardt and Köhler (2015b)

$$s_{OBD,i}^{norm}(t) = 1 + \sum_{j=1}^{2} M_{ij} \, f_{OBD,j}(t) \qquad (2)$$

Fig. 1 The five phase-shifted images of an image stack, from which the wrapped and the unwrapped phase fields are computed. The vertical dashed green line indicates the column shown in Fig. 2. Cell 2, run 2, image stack 60, MR-laser, $T = 25\,°C$
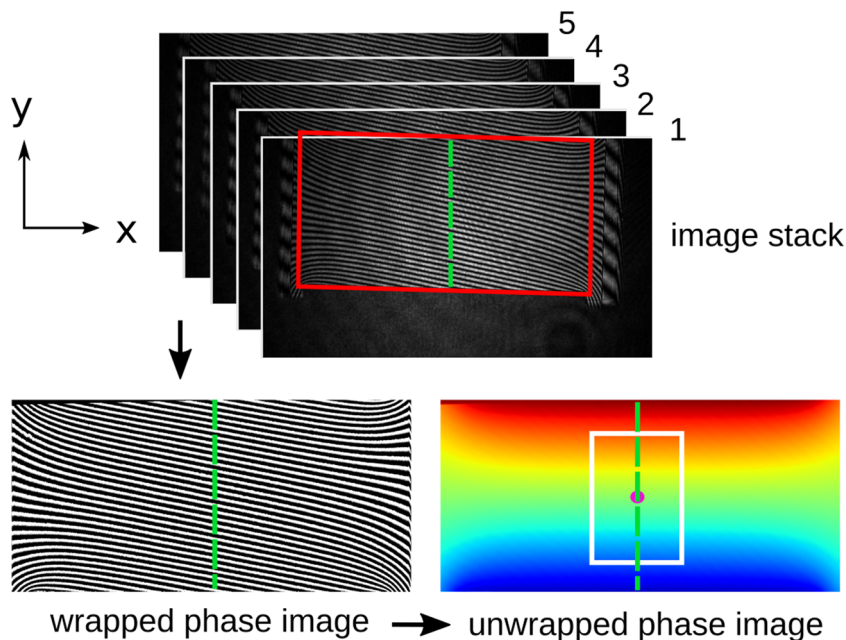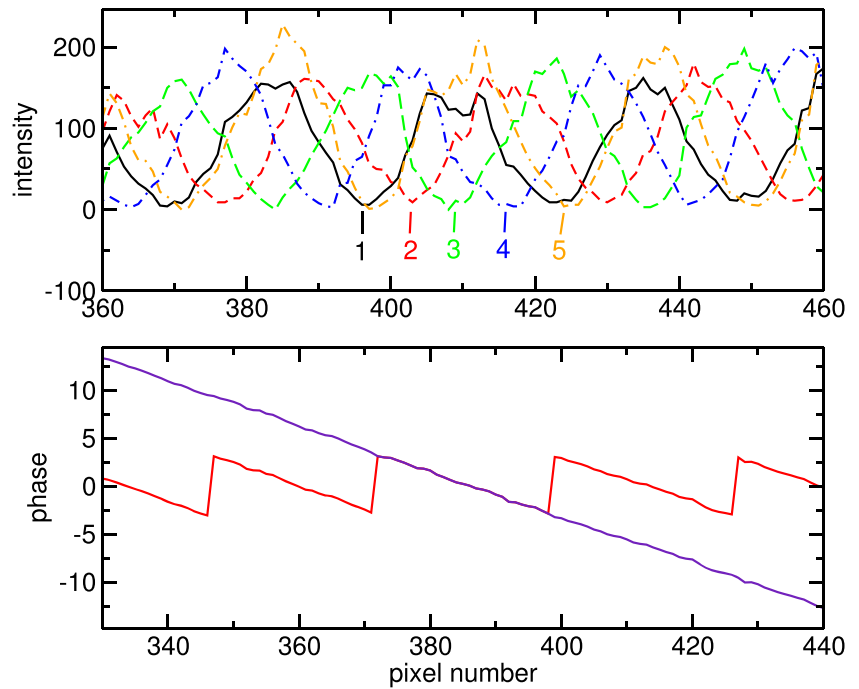

wrapped phase image → unwrapped phase image

Fig. 2 Intensities of the five phase-shifted images plotted along the column marked in Fig. 1. The numbers 1 - 5 refer to the image number within the stack (top). Below are the wrapped and unwrapped phase signals. Cell 2, run 2, image stack 60, MR-laser, $T = 25\,°C$

with

$$
\begin{aligned}
f_{\text{OBD},j}(t) = 1 &+ \frac{1}{2} \sum_{n=-N}^{N} (-1)^n \left[\text{erf}\left(\frac{2\tilde{z} - 2n - 1}{4\sqrt{\tilde{t}_j}} \right) \right. \\
&\left. - \text{erf}\left(\frac{2\tilde{z} - 2n + 1}{4\sqrt{\tilde{t}_j}} \right) \right] \\
&+ \sum_{n=-N}^{N} (-1)^n \frac{1}{4\sqrt{\pi \tilde{t}_j}} \left[\exp\left(-\frac{(2\tilde{z} - 2n + 1)^2}{16\tilde{t}_j} \right) \right. \\
&\left. + \exp\left(-\frac{(2\tilde{z} - 2n - 1)^2}{16\tilde{t}_j} \right) \right].
\end{aligned} \tag{3}
$$

The fit by Eq. 2 contains six unknown parameters: the four entries M_{ij} of the 2×2 amplitude matrix $\underline{\underline{\mathbf{M}}}$, and the two eigenvalues $\hat{D}_i$ of the diffusion matrix, which appear in the dimensionless time $\tilde{t}_j = t/(h^2/\hat{D}_j)$ together with the spacing h between the cold and the hot plate. Averaging over the Gaussian intensity profile of the readout laser beam, as necessary in the case of the true 2-OBD experiments, is not required for the SODI data. With the help of the contrast factor matrices $\underline{\underline{\mathbf{N_c}}}$ and $\underline{\underline{\mathbf{N_T}}}$, defined by $(N_c)_{ij} = (\partial n_i / \partial c_j)_{p,T,c_{k \neq j}}$ and $(N_T)_{ij} = (\partial n_i / \partial T)_{p,c_1,c_2} \delta_{ij}$, the Soret coefficients $\underline{S_T} =$

$(S_{T,1}, S_{T,2})^T$ and the thermodiffusion coefficients $\underline{D_T} = (D_{T,1}, D_{T,2})^T$ are obtained (Gebhardt and Köhler 2015b):

$$
\underline{D'_T} = -\underline{\underline{\mathbf{N_c}}}^{-1} \, \underline{\underline{\mathbf{N_T}}} \, \underline{\underline{\mathbf{M}}} \, \underline{\underline{\hat{\mathbf{D}}}} \, \underline{1} \tag{4}
$$

$$
\underline{S'_T} = -\underline{\underline{\mathbf{N_c}}}^{-1} \, \underline{\underline{\mathbf{N_T}}} \, \underline{\underline{\mathbf{M}}} \, \underline{1} . \tag{5}
$$

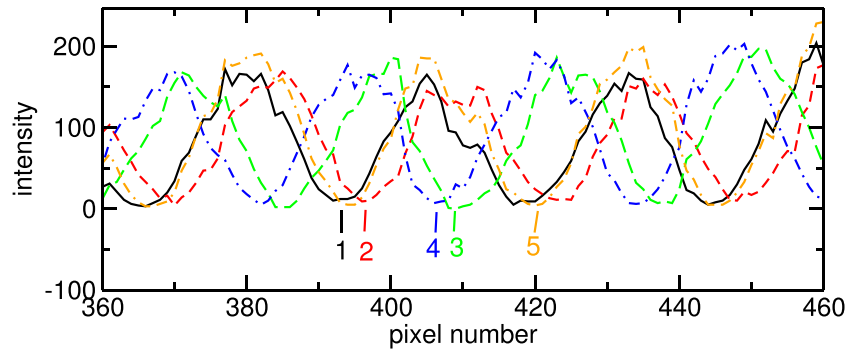Here, $\underline{\underline{\hat{\mathbf{D}}}}$ is the diagonalized diffusion matrix and $\underline{1} = (1, 1)^T$. An example with fits to the beam deflection-like signals of run 2 of the DCMIX3 campaign can be found in Ref. Triller et al. (2019), Fig. 2.

Single-image Fringe Analysis

In case of laser instabilities, the individual images still show interference fringes with reasonable contrast, but the phase stepping becomes erratic. Figure 3 shows, similar to Fig. 2, the fringes along one particular column for the five phase-shifted images of a stack. From a comparison of the two figures, the problem resulting from the instability is evident. Whereas the oscillations in Fig. 2 are nicely shifted by 90 degrees from image to image, the phases in Fig. 3 are more erratic, with some phase steps being much smaller and some much larger than the required 90 degrees.

Under these circumstances, the computation of the wrapped phase image and, thus, the entire temporal phase

stepping approach become inapplicable. In the following, we will discuss an alternative strategy, where the central phase gradient is determined directly from the fringes of every single image and the measurement is mapped to an equivalent 2-OBD-experiment without computation of the phase fields from the image stack.

In principle, the central phase gradient can be determined from the single-image fringe intensity along the y-axis in a straight forward manner by fitting a cosine function with a polynomial $P(y)$ of grade n for the phase:

$$I(y) = A + B\cos(P(y)) \tag{6}$$

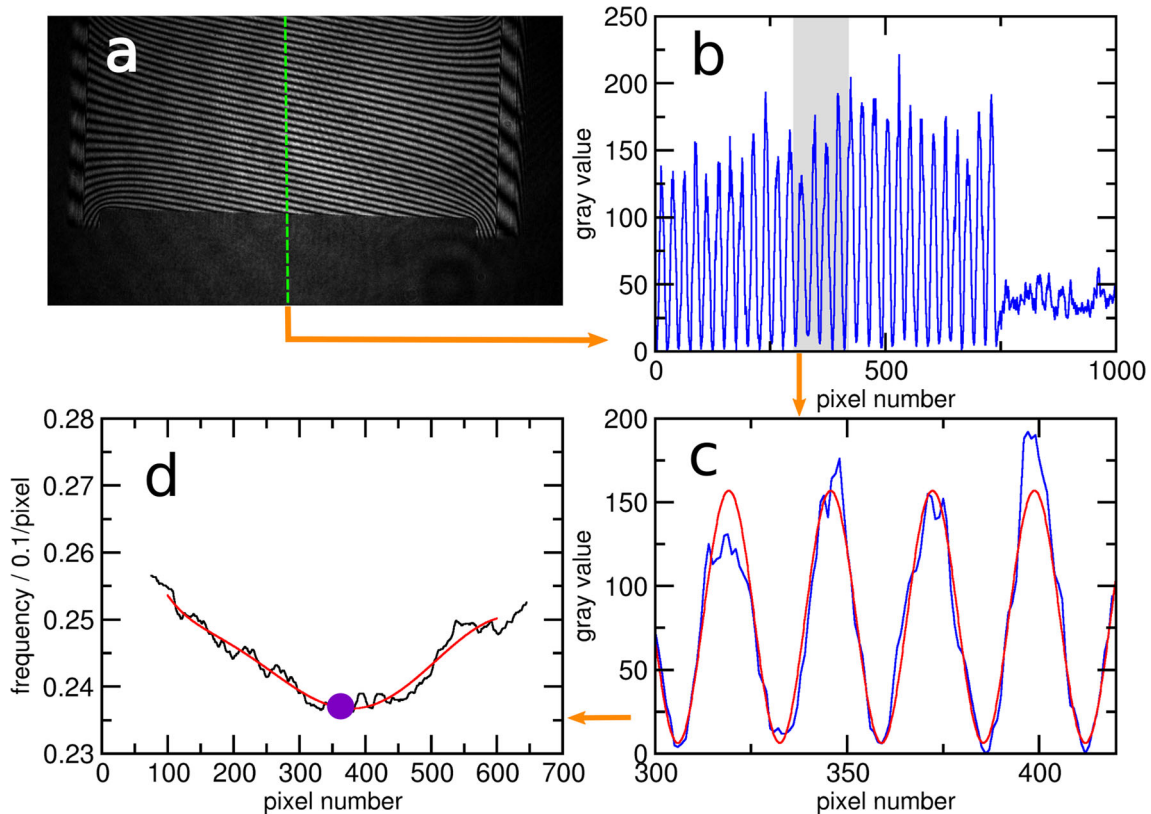$$P(y) = \sum_{i=0}^{n} a_i (y - y_0)^i \tag{7}$$

Fig. 4 Fringe intensity (**b**) along a vertical column through the interference pattern recorded by the SODI camera (**a**). A cosine function with a constant spatial frequency is fitted within a narrow window (**c**). The spatial frequency is plotted as a function of the central position of the window and fitted by a polynomial to determine the phase gradient in the center of the cell (**d**). Cell 2, run 2, image stack 60, image 3, MR-laser, $T = 25\,°C$

Fig. 5 Fringe pattern along column from Fig. 4 with fit of fourth order polynomial (**a**). Determination of the sign changes after subtraction of the fitted polynomial (**b**). Phase plot with seventh order polynomial fit in order to determine the phase gradient in the center of the cell, marked by the dashed vertical line (**c**). The s-shaped dashed curve in (**c**) corresponds to a time before the temperature gradient has reached its stationary value. Cell 2, run 2, image stack 60, image 3, MR-laser, $T = 25\,°C$
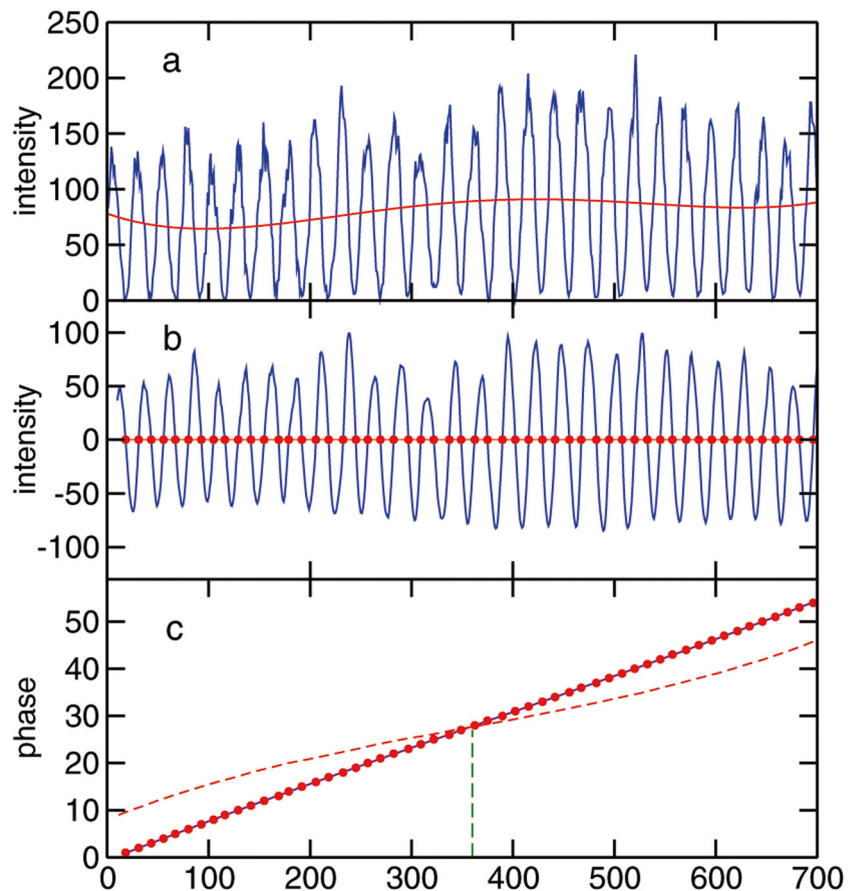
If y_0 is centered at half height between the two plates, the central phase gradient is directly given by the fit parameter a_1.

A fit of Eq. 6 to the fringes along a column, shown in Fig. 4b, would directly yield the solution. It is, however, in practice not feasible for mainly two reasons. First, the convergence of a fit of a cosine function over many periods is rather poor and gets easily trapped in a local minimum. This makes an automated evaluation without human intervention very difficult. Secondly, neither the offset A nor the amplitude B are constant over the height of the cell. Allowing both quantities to vary with y would introduce an undue number of additional fit parameters, which would render the fit even more unstable.

Cosine Method

One way to cope with these problems is sketched in Fig. 4c, where a cosine function $I(y) = A + B\cos(a_0 + a_1 y)$ with a constant spatial frequency is fitted over only short sections of the oscillating fringes. This window is then shifted along the y-axis. The fitted frequencies are plotted in Fig. 4d at the center positions of the respective intervals. These data are further averaged by approximating a suitable

smooth function, e.g., a low order polynomial, which is then evaluated at the center of the cell at $y = y_0$.

Method of Zeros

Instead of fitting short sections of the fringes, the phase gradient can alternatively be obtained from the zero-crossings of the cosine. In a first step the oscillations $I(y)$ are smoothed and made symmetrical to the y-axis by subtracting a proper baseline obtained from a fit of a low order polynomial to the high-frequency fringes (Fig. 5). Sign changes of these symmetric oscillations $\tilde{I}(y)$ occur between row i and $i + 1$, if $I(y_i) \cdot I(y_{i+1}) < 0$. Sub-pixel resolution for the zero-crossings y_0 is obtained from a linear interpolation

$$y_0 = y_i + \left| \tilde{I}(y_i)\, \frac{y_{i+1} - y_i}{\tilde{I}(y_{i+1}) - \tilde{I}(y_i)} \right| . \tag{8}$$

When iterating through the rows, the found zero-crossings $y_{0,k}$ are collected in an array of y-values, and the corresponding phase value is set to $k\pi$, thus constructing the phase that can be fitted by $P(y)$ according to Eq. 7. As before, the central phase gradient is given by the fit parameter a_1.

Fig. 6 Normalized OBD-like signals as obtained by temporal phase-stepping and the two methods that are based on the spatial fringe pattern of single images (cosine method and method of zeros). All signals have been evaluated from a 701 × 201 (rows × columns) region of interest and are normalized to the thermal amplitude. The dashed curve is a fit of Eq. 2 to the curve evaluated by the method of zeros. The residues are shown below the main plot. Cell 2, run 2, $T = 25\,°C$, MN laser (MR laser similar, not shown)
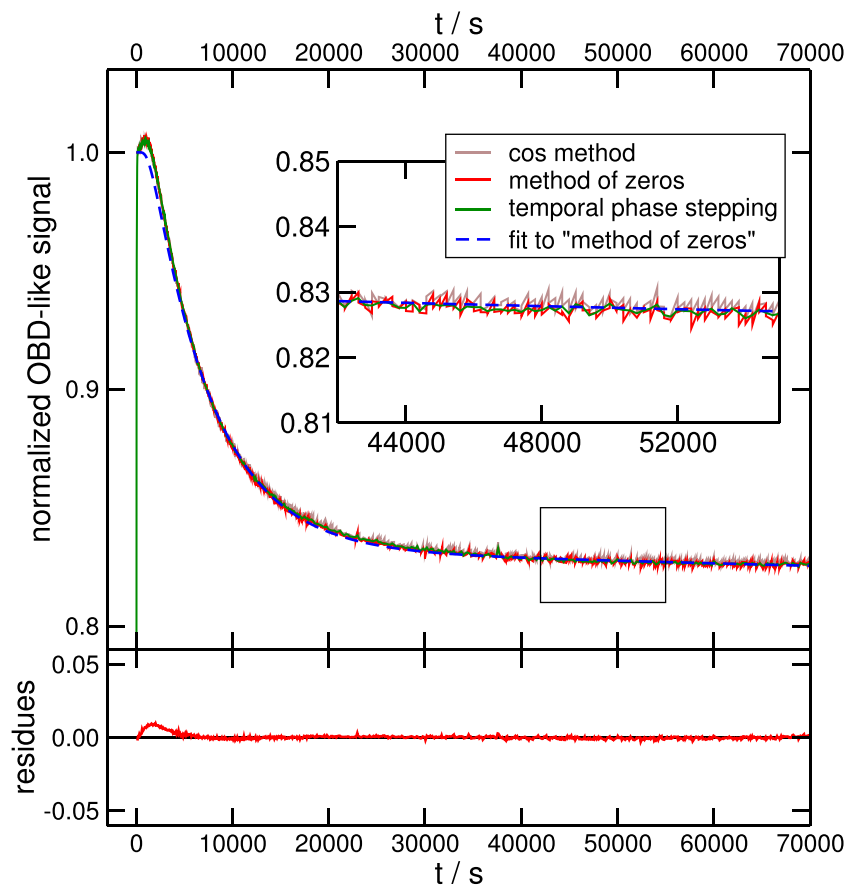
The situation shown in Fig. 5 corresponds to the time where the temperature gradient has reached its stationary value but the concentration gradient has not yet developed. Also shown in Fig. 5c is the s-shaped curve recorded immediately after the temperature step, where the gradient has reached its stationary value near the walls but not yet in the center. Both for the cosine fits and for the zero-crossings, the signal-to-noise ratio is significantly improved by averaging over a larger number of columns, similar to the averaging performed in the temporal phase stepping approach.

Comparison

The OBD-like signals as obtained by the traditional temporal phase-stepping technique and by the two methods based on spatial single-image analysis are compared in Fig. 6. The agreement between all three curves, which are almost indistinguishable, is excellent. In the case of single-image analysis, all images have been evaluated individually and the results for images with identical timestamps have been averaged. In principle, the evaluation of a single image per stack would also be sufficient at the expense of somewhat increased noise.

Also shown in Fig. 6 is, as an example, a fit of Eq. 2 to the curve obtained by the method of zeros. In particular for longer times, the fit perfectly recovers the steady state amplitude, which is important for the determination of the Soret coefficients. Only at very short times, there is a slight overshoot of the experimental data, which is not reproduced by the fit and whose origin is not yet clear.

A decisive test of the performance of the new evaluation method is the quality of the obtained Soret coefficients. Ideally suited for a comparison is cell 2 of DCMIX3 at $25\,°C$, for which not only the microgravity but also ground based 2-OBD and thermogravitational column (TGC) data are available (Triller et al. 2019). The results are shown in Fig. 7 for the two independent components water and ethanol. The upper and the lower part present the results as obtained by the method of zeros and by temporal phase stepping, respectively. Shown are all four runs (2, 7, 12, 17, coded by color) evaluated over three different numbers of vertical columns (51, 201, 1001, coded by shape). The Soret coefficients have been calculated from the amplitude matrix obtained from a fit of Eq. 2 and from the optical contrast factors according to Eq. 5. The thermal optical contrast factors are from Ref. (Triller et al. 2019) and the solutal ones from Ref. (Sechenyh et al. 2011).

Fig. 7 Evaluation of all runs (color coded) for DCMIX3 cell 2 at 25°C by method of zeros (top) and temporal phase stepping (bottom). Averaging over 51, 201, and 1001 columns (coded by shape). Confidence ellipses resulting from one percent Gaussian noise of amplitudes and contrast factors (N_c). Ground based 2-OBD and TGC results from Ref. Triller et al. (2019)
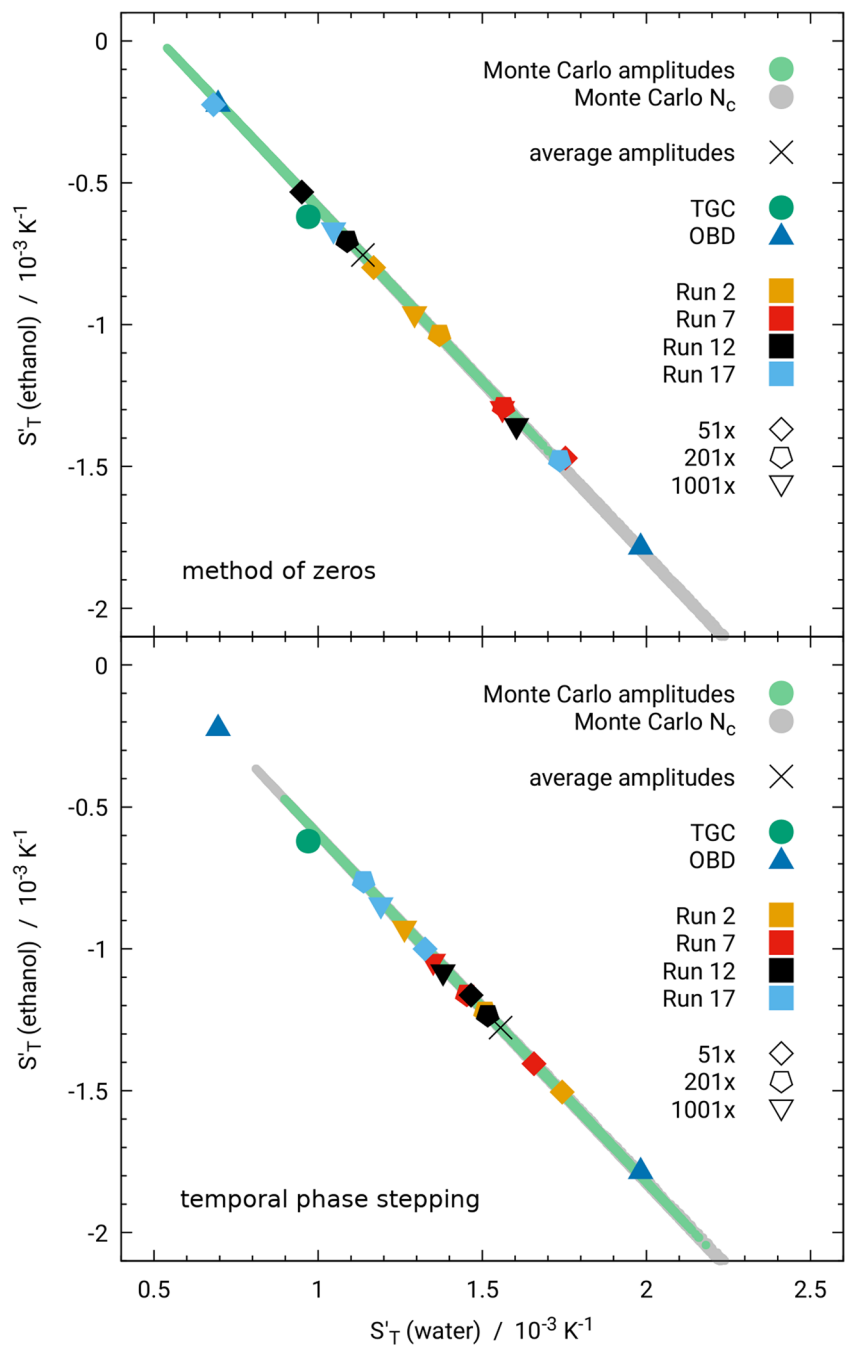

Also shown are 2-OBD and TGC results. The very elongated ellipses are obtained from Monte Carlo simulations with one percent Gaussian noise on the mean amplitudes extracted from the OBD-like SODI signals and on the solutal optical contrast factors. These ellipses represent the confidence regions for the Soret coefficients with an assumed uncertainty of one percent of the directly measurable quantities. Their large extension along the long axis is a direct consequence of the relatively large condition number of the contrast factor matrix. The scatter in the direction of the short axis is only negligible, which is an indication for strongly correlated errors (see Ref. Triller et al. (2019) for details). Most important: practically all data from the SODI, 2-OBD, and TGC measurements are found within these confidence regions, meaning that all results are consistent and agree within experimental error. The similarity between the upper and the lower part of Fig. 7 proves the equivalence of our new single-image based evaluation method and the temporal phase stepping approach that relies on all five images of every image stack.

The final litmus test is the evaluation of a run that is heavily affected by laser instabilities. One such run is run

Fig. 8 Evaluation of run affected by laser instabilities. Temporal phase stepping randomly oscillates between positive and negative values. Correct time trace for method of zeros. Cell 5, run 5, MR-laser, $T = 25\,°C$
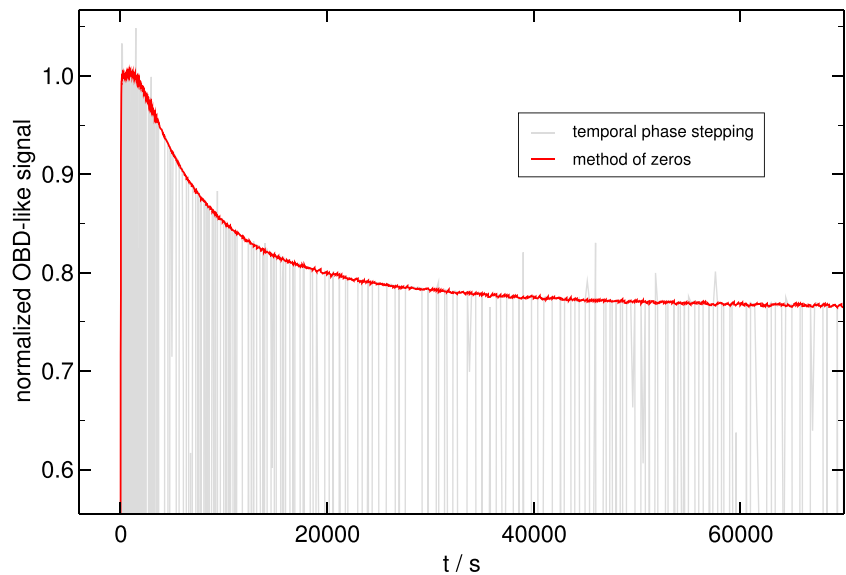
5 (cell 5, MR laser), where the temporal phase stepping approach completely fails (Triller et al. 2018). As shown in Fig. 8, some stacks can still be treated by temporal phase stepping, but half of them yield phase shifts that are completely off, resulting in a time trace that randomly oscillates between positive and negative values (gray curve). This behavior renders automated evaluation by temporal phase stepping impossible. The evaluation based on single-image fringe analysis, however, works perfectly without a single outlier and yields a perfect OBD-like transient.

Summary and Conclusions

We have introduced a new data evaluation method for the DCMIX experiments that is based on the analysis of single individual images of the interference fringes. By determining the phase gradient in the center of the cell, the SODI measurements can be mapped onto equivalent 2-OBD experiments. Although not all information contained in the 2d-images is utilized, this mapping of the SODI experiments has the advantage that the further analysis of the transient signals can be performed according to the well established optical beam deflection procedures (Haugen and Firoozabadi 2006; Piazza and Guarino 2002; Königer et al. 2010).

Under normal circumstances with properly working temporal phase stepping, this method merely provides an attractive alternative way to extract the diffusion, thermal diffusion and Soret coefficients from the microgravity experiments. The biggest advantage can be drawn in situations with laser instabilities and not properly working

temporal phase stepping. Such instabilities occur from time to time in the SODI instrument, and so far their origin could not be identified. It is also not possible to repair the instrument, which is permanently stored aboard the ISS, by, e.g., exchanging the lasers. Since these perturbations occur only sporadic, they have not yet led to severe losses of data. Given the efforts necessary to perform experiments under microgravity conditions, it is, however, desirable to extract as much information as possible and to evaluate also the runs affected by perturbations.

Our new method to extract the central phase gradient from the spatial fringe patterns of a single image instead from the combination of all five phase-shifted images within a stack closes exactly this gap. The transients obtained by this alternative analysis are of similar quality as the ones determined by the traditional phase stepping approach. Even for measurements without phase perturbations, the method can serve as a convenient cross check of the results obtained by other evaluation schemes.

The new method is robust, since it can be applied to all image stacks, no matter whether they are affected by laser instabilities or not. It also proves the robustness of the entire SODI instrument, which is capable of delivering high quality data even in situations where central components of the interferometer fail to work as designed. In principle, it should also be possible to evaluate these malformed image stacks by the Fourier transform method (Khlybov et al. 2015), but this has not yet been investigated in detail.

References

Ahadi, A., Varenbergh, S.V., Saghir, M.Z.: J. Chem. Phys. **138**, 204201 (2013). https://doi.org/10.1063/1.4802984

Ahadi, A., Ziad Saghir, M.: Eur. Phys. J. E **38**, 25 (2015). https://doi.org/10.1140/epje/i2015-15025-4

Bou-Ali, M.M., Ahadi, A., de Mezquia, D.A., Galand, Q., Gebhardt, M., Khlybov, O., Köhler, W., Larrañaga, M., Legros, J.C., Lyubimova, T., Mialdun, A., Ryzhkov, I., Saghir, M.Z., Shevtsova, V., Vaerenbergh, S.V.: Eur. Phys. J. E **38**, 30 (2015). https://doi.org/10.1140/epje/i2015-15030-7

de Mezquia, D.A., naga, M.L., Bou-Ali, M.M., Madariaga, J.A., Santamaria, C., Platten, J.K.: Int. J. Thermal Sci. **92**, 14 (2015). https://doi.org/10.1016/j.ijthermalsci.2015.01.013

Galand, Q., Van Vaerenbergh, S.: Eur. Phys. J. E **38**, 26 (2015). https://doi.org/10.1140/epje/i2015-15026-3

Gebhardt, M., Köhler, W.: Eur. Phys. J. E **38**, 24 (2015a). https://doi.org/10.1140/epje/i2015-15024-5

Gebhardt, M., Köhler, W.: J. Chem. Phys. **142**, 084506 (2015b). https://doi.org/10.1063/1.4908538

Gebhardt, M., Köhler, W.: J. Chem. Phys. **143**, 164511 (2015c). https://doi.org/10.1063/1.4934718

Haugen, K.B., Firoozabadi, A.: J. Phys. Chem. B **110**, 17678 (2006). https://doi.org/10.1021/jp062382m

Jurado, R., Gavalda, J., Simon, M.J., Pallares, J., Laveron-Simavilla, A., Ruiz, X., Shevtsova, V.: Acta Astronaut. **129**, 345 (2016). https://doi.org/10.1016/j.actaastro.2016.09.033

Jurado, R., Pallares, J., Gavalda, J., Ruiz, X.: Int. J. Thermal Sci. **132**, 186 (2018). https://doi.org/10.1016/j.ijthermalsci.2018.05.040

Khlybov, O.A., Ryzhkov, I.I., Lyubimova, T.P.: Eur. Phys. J. E **38**, 29 (2015). https://doi.org/10.1140/epje/i2015-15029-0

Köhler, W., Morozov, K.I.: J. Non-Equilib. Thermodyn. **41**, 151 (2016). https://doi.org/10.1515/jnet-2016-0024

Königer, A., Wunderlich, H., Köhler, W.: J. Chem. Phys. **132**, 174506 (2010). https://doi.org/10.1063/1.3421547

Kreis, T.: Handbook of Holographic Interferometry: Optical and Digital Methods. Wiley, Hoboken (2005)

Larrañaga, M., Bou-Ali, M.M., de Mezquia, D.A., Rees, D.A.S., Madariaga, J.A., Santamaria, C., Platten, J.K.: Eur. Phys. J. E **38**, 28 (2015). https://doi.org/10.1140/epje/i2015-15028-1

Legros, J.C., Gaponenko, Y., Mialdun, A., Triller, T., Hammon, A., Bauer, C., Köhler, W., Shevtsova, V.: Phys. Chem. Chem. Phys. **17**, 27713 (2015). https://doi.org/10.1039/C5CP04745E

Mialdun, A., Legros, J.C., Yasnou, V., Sechenyh, V., Shevtsova, V.: Eur. Phys. J. E **38**, 27 (2015). https://doi.org/10.1140/epje/i2015-15027-2

Mialdun, A., Minetti, C., Gaponenko, Y., Shevtsova, V., Dubois, F.: Microgravity Sci. Tec. **25**, 83 (2013). https://doi.org/10.1007/s12217-012-9337-2

Mialdun, A., Ryzhkov, I., Khlybov, O., Lyubimova, T., Shevtsova, V.: J. Chem. Phys. **148**, 044506 (2018). https://doi.org/10.1063/1.5017716

Mounir, B.A.S.M., Platten, J.K.: J. Non-Equilib. Thermodyn. **30**, 385 (2005). https://doi.org/10.1515/JNETDY.2005.027

Ollé, J., Dubert, D., Gavaldà, J., Laveron-Simavilla, A., Ruiz, X., Shevtsova, V.: Acta Astronaut. **140**, 409 (2017). https://doi.org/10.1016/j.actaastro.2017.09.007

Pearlstein, A.J., Harris, R.M., Terrones, G.: J. Fluid Mech. **202**, 443 (1989). https://doi.org/10.1017/S0022112089001242

Piazza, R., Guarino, A.: Phys. Rev. Lett. **88**, 208302 (2002). https://doi.org/10.1103/PhysRevLett.88.208302

Platten, J.K., Legros, J.C.: Convection in Liquids. Springer, Heidelberg (1984)

Sechenyh, V., Legros, J.C., Shevtsova, V.: J. Chem. Thermodyn. **43**, 1700 (2011). https://doi.org/10.1016/j.jct.2011.05.034

Shevtsova, V., Sechenyh, V., Nepomnyashchy, A., Legros, J.C.: Philos. Mag. **91**, 3498 (2011). https://doi.org/10.1080/14786435.2011.586376

Shevtsova, V., Santos, C., Sechenyh, V., Legros, J.C., Mialdun, A.: Microgravity Sci. Tec. **25**, 275 (2014). https://doi.org/10.1007/s12217-013-9349-6

Touzet, M., Galliero, G., Lazzeri, V., Saghir, M.Z., Montel, F., Legros, J.C.: CR Mecanique **339**, 318 (2011). https://doi.org/10.1016/j.crme.2011.03.008

Triller, T.: Diffusive Properties of the System Water/Ethanol/Triethylene Glycol in Microgravity and Ground Conditions. Ph.D. thesis, Universität Bayreuth. https://epub.uni-bayreuth.de/3861/ (2018)

Triller, T., Bataller, H., Bou-Ali, M.M., Braibanti, M., Croccolo, F., Ezquerro, J.M., Galand, Q., Gavaldà, J., Lapeira, E., Laverón-Simavilla, A., Lyubimova, T., Mialdun, A., de Zárate, J.M.O., Rodríguez, J., Ruiz, X., Ryzhkov, I.I., Shevtsova, V., Vaerenbergh, S.V., Köhler, W.: Microgravity Sci. Tec. **30**, 295 (2018). https://doi.org/10.1007/s12217-018-9598-5

Triller, T., Sommermann, D., Schraml, M., Sommer, F., Lapeira, E., Bou-Ali, M.M., Köhler, W.: vol. 42. https://doi.org/10.1140/epje/i2019-11789-7. https://rdcu.be/bpGYk (2019)

Vaerenbergh, S.V., Garandet, J.P., Praizey, J.P., Legros, J.C.: Phys. Rev. E **58**, 1866 (1998). https://doi.org/10.1103/PhysRevE.58.1866

Van Vaerenbergh, S., Legros, J.C., Dupin, J.C.: Adv. Space Res. **16**, 69 (1995). https://doi.org/10.1016/0273-1177(95)00273-H

Van Vaerenbergh, S., Legros, J.C.: J. Phys. Chem. B **102**, 4426 (1998). https://doi.org/10.1021/jp9802329

Wiegand, S.: J. Phys.: Condens. Matter **16**, R357 (2004). https://doi.org/10.1088/0953-8984/16/10/R02